Journal of Catalysis **189,** 281–296 (2000)
doi:10.1006/jcat.1999.2723, available online at http://www.idealibrary.com on IDEAL®

Zeolite-Supported Ni and Mo Catalysts for Hydrotreatments

II. HRTEM Observations

Dien Li,*[,1] Huifang Xu,† and George D. Guthrie, Jr.*

*Earth and Environment Sciences Division, Los Alamos National Laboratory, Los Alamos, New Mexico 87545; and †Department of Earth & Planetary Sciences, The University of New Mexico, Albuquerque, New Mexico 87131

Received April 21, 1999; revised October 4, 1999; accepted October 11, 1999

Calcined and sulfided Ni–Mo catalysts supported on ultrastable Y zeolite (USY), NaY zeolite, mordenite, and ZSM-5 were studied by high-resolution electron transmission microscopy (HRTEM) with selected-area electron diffraction (SAED) and energy-dispersive spectroscopy (EDS). Ni and Mo oxide aggregates were rarely observed in the USY-supported Ni–Mo catalyst, indicating that most of Ni and Mo may be incorporated into USY, e.g., supercavities and possibly sodalite cages. However, there were a large number of α-$NiMoO_4$ aggregates of different particle sizes in NaY-, mordenite-, and ZSM-5-supported catalysts, and the mordenite-supported catalyst also contained MoO_3 crystals. The α-$NiMoO_4$ may be attached to the surface of substrates as individual particles or needle aggregates, it may be disseminated into mordenite particles, or it may even form an isolated sphere (in Ni–Mo/NaY) or a needle (in Ni–Mo/ZSM-5) aggregates. Thus, most of Ni and Mo in NaY-, mordenite-, and ZSM-5-supported catalysts preferentially formed aggregates, although some Mo may have been incorporated into NaY and ZSM-5. After sulfidation, small MoS_2 aggregates containing some Ni were rarely but occasionally found on the surface of USY zeolite; however, there were a large number of such MoS_2 aggregates on the surface of NaY. Separate and intergrown MoS_2 and Ni sulfides aggregates were observed on the surface of mordenite and ZSM-5. The Ni sulfide might be identified by SAED and high-magnification images as troilite-like NiS and/or Ni_9S_8, but definitely not as NiS with millerite structure or Ni_3S_2. These results indicated that sulfidation does not extensively affect Ni and Mo that have been incorporated into the supercavity and/or sodalite cage of USY in calcined Ni–Mo/USY. After sulfidation, Ni–Mo sulfide species may have formed in the supercavity and possibly in the sodalite cage of the USY zeolite. However, in NaY-, mordenite-, and ZSM-5-supported Ni–Mo catalysts, Ni and Mo may have predominantly formed Ni–Mo sulfides or even separate Mo and Ni sulfide phases on the surface of the substrates. Thus, the USY-supported Ni–Mo catalyst had a much higher hydrodesulfurization (HDS) activity than the other zeolite-supported catalysts, which is attributed to both the highly dispersed Ni and/or Mo sulfide species in supercavities and possibly in sodalite cages of a USY zeolite, and the presence of Brønsted acidity in a USY zeolite we have demonstrated previously (Li, Dien, Nishijima, A., and Morris, D. E., *J. Catal*. 182, 339 (1999)).

Key Words: **ultrastable Y zeolites; Ni–Mo oxides; Ni–Mo sulfides; hydrodesulfurization; environmental catalysis; high-resolution transmission electron microscopy.**

INTRODUCTION

Zeolites have been applied extensively as solid-acid catalysts for decades. However, over the last decade, much attention has also been given to the application of zeolites as substrates for transition-metal catalysts used in hydrotreating (1) because of their acidity, shape selectivity, and resistance to poisoning by sulfur and nitrogen. For example, the catalytic activity of Ni(Co)–Mo sulfide catalysts supported on zeolites has been studied for hydrocracking (HC) of *n*-heptane (2), alkanes (3), and *n*-decane (4), for hydrodesulfurization (HDS) of thiophene (5–9), ethylbenzene (10), benzothiophene (11), and gas oil (12), and for hydrogenation of benzene (13–15). A synergistic effect has been reported to occur at a Ni/(Ni + Mo) ratio of about 0.4–0.5. Indeed, transition-metal catalysts supported on zeolites appear to be promising for deep HDS catalysis in the production of clean-burning fuels (16).

In this quest for new generation catalysts for deep HDS of petroleum and liquified coal, we have studied the hydrotreatment potential of zeolite-supported Ni–Mo catalysts. In a previous paper (17), we found that a sulfided Ni–Mo catalyst supported on ultrastable Y zeolite (USY) has very high HDS and HC activity compared with that of similar sulfided Ni–Mo catalysts supported on Na Y zeolite (NaY), mordenite, or ZSM-5. HDS activity in these types of catalysts is known to depend on the formation of Ni–Mo–S phases during sulfidation, which in turn depends on the nature of Ni and Mo in the zeolite-supported Ni–Mo catalyst precursor (before sulfidation) (15). Yet, the nature and distribution of Ni and Mo in these types of Ni–Mo catalyst

[1] To whom correspondence should be addressed. EES-1, MS D462, Los Alamos National Laboratory, Los Alamos, NM 87545. Fax: 1-505-665-3285. E-mail: dienli@lanl.gov.

0021-9517/00 $35.00

precursors remain poorly understood, and the major active Ni and/or Mo sulfide phases responsible for high HDS activity are also controversial.

Transmission electron microscopy (TEM) has been used extensively to study the nature of transition-metal (e.g., Co, Ni, and Mo) sulfide catalysts supported on Al_2O_3 (18–30) and other oxides (31–34). The zeolite-supported Ni, Mo, and Ni–Mo catalysts have also been studied by TEM, but the TEM results from different groups are not fully consistent. For example, Cid *et al.* (35) found no clear evidence for the presence of a MoO_3 phase in NaY-supported Mo catalysts containing up to 15 wt% MoO_3. Leglise *et al.* (13–15) showed that all of the Ni species and more than half of the Mo species were found in HY zeolite cavities, and MoO_3 was also observed outside the zeolite grain. The sulfidation transforms the outside MoO_3 into MoS_2 and evicts about 50% of Ni to form a Ni–Mo–S phase in zeolite mesopores, and the Ni–Mo sulfide in the zeolite is highly dispersed and responsible for the high hydrogenation activity of benzene (13–15). However, Welters *et al.* (36–38) argued that the very small Ni and Mo sulfide clusters located in the NaY supercavities strongly contribute to the thiophene HDS activity and that no promoter effect is observed in the hydrocracking of *n*-decane over Ni–Mo/NaY.

The nature and distribution of Ni and Mo in the calcined catalysts are closely related to the sulfidation extent, the dispersion of active-metal phases, and catalytic activity. Thus, we studied the nature and distribution of Ni and Mo in both calcined and sulfided Ni–Mo catalysts supported on USY, NaY, mordenite, and ZSM-5 using high-resolution transmission electron microscopy (HRTEM) with selected-area electron diffraction (SAED) and energy-dispersive spectroscopy (EDS). We investigated the following questions: (1) What are the nature and distribution of Ni and Mo in calcined Ni–Mo catalyst precursors? For example, what is the relative proportion of Ni and Mo preferentially distributed on the surface of zeolites versus Ni and Mo within zeolites and what are the entities of Ni–Mo phases that form on the surface of zeolites? (2) What are the nature and distribution of Ni and Mo in sulfided Ni–Mo catalysts? (3) What is the relationship between the nature of Ni and Mo in the zeolite and catalytic HDS activity?

EXPERIMENTAL

Catalyst Preparation

NaY, USY, and ZSM-5 were provided by Catalysts & Chemicals Industry Ltd. (Japan), and H-mordenite was obtained from Tosoh (Japan). NaY was ion-exchanged with $(NH_4)_2SO_4$ solution to prepare the NH_4 form of the zeolite, which was calcined at 550°C for 1 h to obtain HY zeolite. The HY zeolite was steamed at 700°C for 3 h for dealumination and then washed using an aqueous solution of H_2SO_4 (pH 2.7) to prepare USY. USY, NaY, mordenite, and ZSM-5 (10 g) were used to prepare zeolite-supported Ni–Mo catalysts by conventional ion exchange of the aqueous solutions at about 60°C for 2 h. The aqueous solutions were prepared by dissolving $(NH_4)_6Mo_7O_{24} \cdot 4H_2O$ (0.98 g) and $Ni(NO_3)_2 \cdot 6H_2O$ (0.78 g) in distilled water (15 ml) with additional aqueous ammonia (6 ml), so that the ideal concentrations of NiO and MoO_3 in the final catalysts were 2 and 8 wt% with a molar NiO/MoO_3 ratio of about 0.48. After ion exchange, the aqueous solution was evaporated at about 80°C, and the Ni–Mo/zeolites slurries were dried at 200°C for 2 h in a rotary kiln and calcined at 550°C for 3 h in air. The zeolite-supported Ni–Mo catalyst precursors were sulfided at 400°C for 2 h under a stream of H_2S–H_2 (vol% $H_2S = 5.04$) before the hydrodesulfurization (HDS) activity of dibenzothiophene (DBT) was tested (17). The description and HDS activity of the various zeolites, their supported Ni–Mo precursors, and sulfided catalysts are given in Table 1. The chemical compositions of the calcined Ni–Mo catalyst precursors were determined by irradiated neutron activation analysis (INAA) or by inductively coupled plasma emission spectroscopy (ICP-ES), for comparison with the results analyzed by EDS (Table 2).

High-Resolution Transmission Electron Microscopy

Powder samples of Ni–Mo/USY, Ni–Mo/NaY, Ni–Mo/mordenite, and Ni–Mo/ZSM-5 (which had aged in air at room temperature for about 2 years following preparation and calcination) were deposited on holey-carbon film supported on Cu grids. Specimen were examined using a JEOL 2010 TEM operated at 200 kV (point-to-point resolution = 1.9 Å). Very thin, transparent, and clean zeolite particles were chosen for EDS analysis, so that Ni and Mo detected by EDS within the spot size of about 30 nm can be thought as Ni and Mo in the lattice structure of zeolites. Composition of spots on individual particles were semiquantified assuming a thin-film criterion and experimentally derived Cliff-Lorimer *k* factors for Na $K\alpha$ (using jadeite), Al $K\alpha$ (using jadeite), and Ni $K\alpha$ (using a Ni olivine), and a theoretical *k* factor for Mo $L\alpha$. Mole percents for Na_2O, Al_2O_3, SiO_2, NiO, and MoO_3 were normalized to 100%.

RESULTS

Ni–Mo/USY

A large number of USY particles in calcined Ni–Mo/USY catalyst were surveyed using HRTEM. USY was well-crystallined as indicated by SAED and by conventional bright-field imaging (Fig. 1A). EDS showed the presence of Ni and Mo in the USY particles (Fig. 1D; Table 2). However, Ni and Mo oxide aggregates were rarely found on the

TABLE 1

Description and HDS Activity of Samples Discussed in This Work

Samples	Descriptions	HDS activity %	HDS activity $\times 10^8$ mmol/m$^2 \cdot$ s
Zeolite supports			
USY	$SiO_2/Al_2O_3 = 8.1$; $Na_2O = 10.86$ wt%; BET surface area = 763 m^2/g	12.6	0.14
NaY	$SiO_2/Al_2O_3 = 4.7$; $Na_2O = 0.31$ wt%; BET surface area = 759 m^2/g	7.7	0.09
Mordenite	$SiO_2/Al_2O_3 = 14.7$; $Na_2O = 0.39$ wt%; BET surface area = 524 m^2/g	5.5	0.09
ZSM-5	$SiO_2/Al_2O_3 = 166.4$; $Na_2O = 0.03$ wt%; BET surface area = 408 m^2/g	5.7	0.12
Ni–Mo catalyst precursors			
Ni–Mo/USY	Prepared by ion exchange of Ni–Mo solution; dried at 200°C for 2 h; calcined at 550°C for 3 h		
Ni–Mo/NaY	Prepared by ion exchange of Ni–Mo solution; dried at 200°C for 2 h; calcined at 550°C for 3 h		
Ni–Mo/mordenite	Prepared by ion exchange of Ni–Mo solution; dried at 200°C for 2 h; calcined at 550°C for 3 h		
Ni–Mo/ZSM-5	Prepared by ion exchange of Ni–Mo solution; dried at 200°C for 2 h; calcined at 550°C for 3 h		
Ni–Mo sulfided catalysts			
Ni–Mo/USY-(S)	Sulfided under a stream of H_2–H_2S mixture (the vol% $H_2S = 5.04$) at 400°C for 2 h	93.7	1.05
Ni–Mo/NaY-(S)	Sulfided under a stream of H_2–H_2S mixture (the vol% $H_2S = 5.04$) at 400°C for 2 h	22.6	0.26
Ni–Mo/mordenite-(S)	Sulfided under a stream of H_2–H_2S mixture (the vol% $H_2S = 5.04$) at 400°C for 2 h	7.2	0.12
Ni–Mo/ZSM-5-(S)	Sulfided under a stream of H_2–H_2S mixture (the vol% $H_2S = 5.04$) at 400°C for 2 h	7.2	0.16

surface of USY particles. As a whole, the evidence suggests that Ni and Mo may be incorporated into extraframework sites of the USY, e.g., the supercavity or possibly the sodalite cage. The only exception was that one single Ni–Mo aggregate of about 50 nm in size was observed on the surface of a USY particle (Fig. 1B). EDS analysis (Fig. 1E) of this aggregate indicated that this was a Ni–Mo oxide aggregate, and the SAED pattern (the inset of Fig. 1B), high-magnification image, and its Fourier transform (Fig. 1C) suggest that this aggregate was a monoclinic α-$NiMoO_4$.

In sulfided Ni–Mo/USY catalyst, Ni–Mo sulfide aggregates on the surface of USY zeolite were rarely but occasionally found (Fig. 2A). EDS (Fig. 2C) showed that Ni, Mo, and possibly S (because the S $K\alpha$ and Mo L line were overlapped in EDS) were present in the USY zeolite within the spot size detected by the electron beam (~30 nm), indicating that Mo and Ni or Ni–Mo sulfide species might have formed within the supercavity and possibly the sodalite cage of USY zeolite. The only one Ni–Mo sulfide aggregate of about 40 nm in size was found (Fig. 2A) after a large number of USY particles were surveyed. The high-magnification image and EDS of this aggregate are shown in Figs. 2B and 2D. This aggregate was spherical and the bending fringes surrounded the whole particle. The d spacing measured from the high-magnification fringes was about 6.4 Å, close to the d_{002} of MoS_2 (6.15 Å). The reason for the bending fringes was unclear yet, but the bending fringes of MoS_2 have been observed in Ni–Mo/Al_2O_3 (26–28) and Ni–Mo/Y zeolite catalysts (15, 36, 37). The quality of the SAED pattern (the inset of Fig. 2B) was poor, in which the (002) line ($d = 6.15$ Å) was not observed due to a large central spot, but the other two broad diffraction lines with d spacings of about 2.35 and 2.14 Å may be indexed as (103) and (006) of MoS_2. A much better quality SAED pattern of MoS_2 in sulfided Ni–Mo/ZSM-5 is shown in Fig. 8C. EDS in Fig. 2D indicated the presence of Mo and a small amount of Ni in this aggregate; a very small amount of O and Si may be due to USY zeolite that supported this aggregate. Because the S $K\alpha$ line and Mo L line were overlapped in EDS, and the catalyst was sulfided under 400°C and atmospheric pressure in which MoS_2 should be the most stable phase, this aggregate might be MoS_2 that contained some Ni (15, 26, 36, 42). Although it was not certain about the precursor of this Ni–Mo sulfide aggregate, its precursor was speculated to be the α-$NiMoO_4$ aggregate in calcined Ni–Mo/USY zeolite. Thus, all results indicate that there was

TABLE 2

Chemical Composition of Zeolite-Supported Ni–Mo Catalyst Precursors

	Ni–Mo/USY			Ni–Mo/NaY		
	ICP/INAA[a] (wt%)	EDS[b] (wt%)	EDS_{corr}[c] (wt%)	ICP/INAA[a] (wt%)	EDS[b] (wt%)	EDS_{corr}[c] (wt%)
SiO_2	75.90	80.90	75.90	58.00	70.20	58.00
Al_2O_3	15.90	14.00	13.13	21.30	23.30	19.25
Na_2O	0.30	0.50	0.47	11.90	2.8	2.31
NiO	1.60	0.70	0.66	1.70	0.10	0.08
MoO_3	6.30	3.90	3.66	7.10	3.60	2.97
NiO/MoO_3	0.49			0.46		
Total	100.00	100.00	93.82	100.00	100.00	82.62
	Mole fraction			Mole fraction		
Si	0.80	0.83	0.83	0.70	0.72	0.72
Al	0.20	0.17	0.17	0.30	0.28	0.28
Na	0.01	0.01	0.01	0.28	0.06	0.06
Ni	0.01	0.01	0.01	0.02	0.00	0.00
Mo	0.04	0.02	0.02	0.05	0.02	0.02
Al + Si	1.00	1.00	1.00	1.00	1.00	1.00
Al/Si	0.25	0.20	0.20	0.43	0.39	0.39
	Ni–Mo/mordenite			**Ni–Mo/ZSM-5**		
	ICP/INAA[a] (wt%)	EDS[b] (wt%)	EDS_{corr}[c] (wt%)	ICP/INAA[a] (wt%)	EDS[b] (wt%)	EDS_{corr}[c] (wt%)
SiO_2	84.30	86.20	84.30	91.60	97.20	91.60
Al_2O_3	9.70	9.20	9.00	0.90	0.00	0.00
Na_2O	0.20	0.10	0.10	0.10	0.00	0.00
NiO	2.10	1.80	1.76	1.50	0.00	0.00
MoO_3	3.70	2.50	2.44	5.90	2.80	2.64
NiO/MoO_3	1.09			0.48		
Total	100.00	99.80	97.60	100.00	100.00	94.24
	Mole fraction			Mole fraction		
Si	0.88	0.89	0.89	0.99	1.00	1.00
Al	0.12	0.11	0.11	0.01	0.00	0.00
Na	0.00	0.00	0.00	0.00	0.00	0.00
Ni	0.02	0.01	0.01	0.01	0.00	0.00
Mo	0.02	0.01	0.01	0.03	0.02	0.02
Al + Si	1.00	1.00	1.00	1.00	1.00	1.00
Al/Si	0.14	0.13	0.13	0.01	0.00	0.00

[a] The bulk compositions were determined for SiO_2, Al_2O_3, and Na_2O by an inductively couple plasma emission spectrometer (ICP-ES) and for NiO and MoO_3 irradiated neutron activation analysis (INAA), excluding hydrogen.

[b] Energy-dispersive spectroscopy (EDS) gave semiquantitative bulk compositions in a microscopic area (~30 nm). The data are means based on the population of the 6–10 points analysed. Precision for EDS data is normally about 5–10% relative to individual analysis.

[c] EDS_{corr} is re-normalized based on the wt% of SiO_2 as determined by ICP. Mole fraction is based on Si + Al = 1.

no evidence to support that Ni and/or Mo in USY were extensively affected by sulfidation.

Ni–Mo/NaY

NaY was crystalline (Fig. 3A), as evidenced by the SAED pattern in the inset. EDS showed that a small amount of Mo was present in the zeolite, but almost no Ni was found in NaY (the inset of Fig. 3A; Table 2). A large number of Ni and Mo aggregates were observed on the surface of NaY (Fig. 3A), and Ni–Mo oxide even formed an isolated spherical aggregate of large size (Fig. 3B). The high-magnification image (Fig. 3C), SAED pattern (the inset of Fig. 3C), and

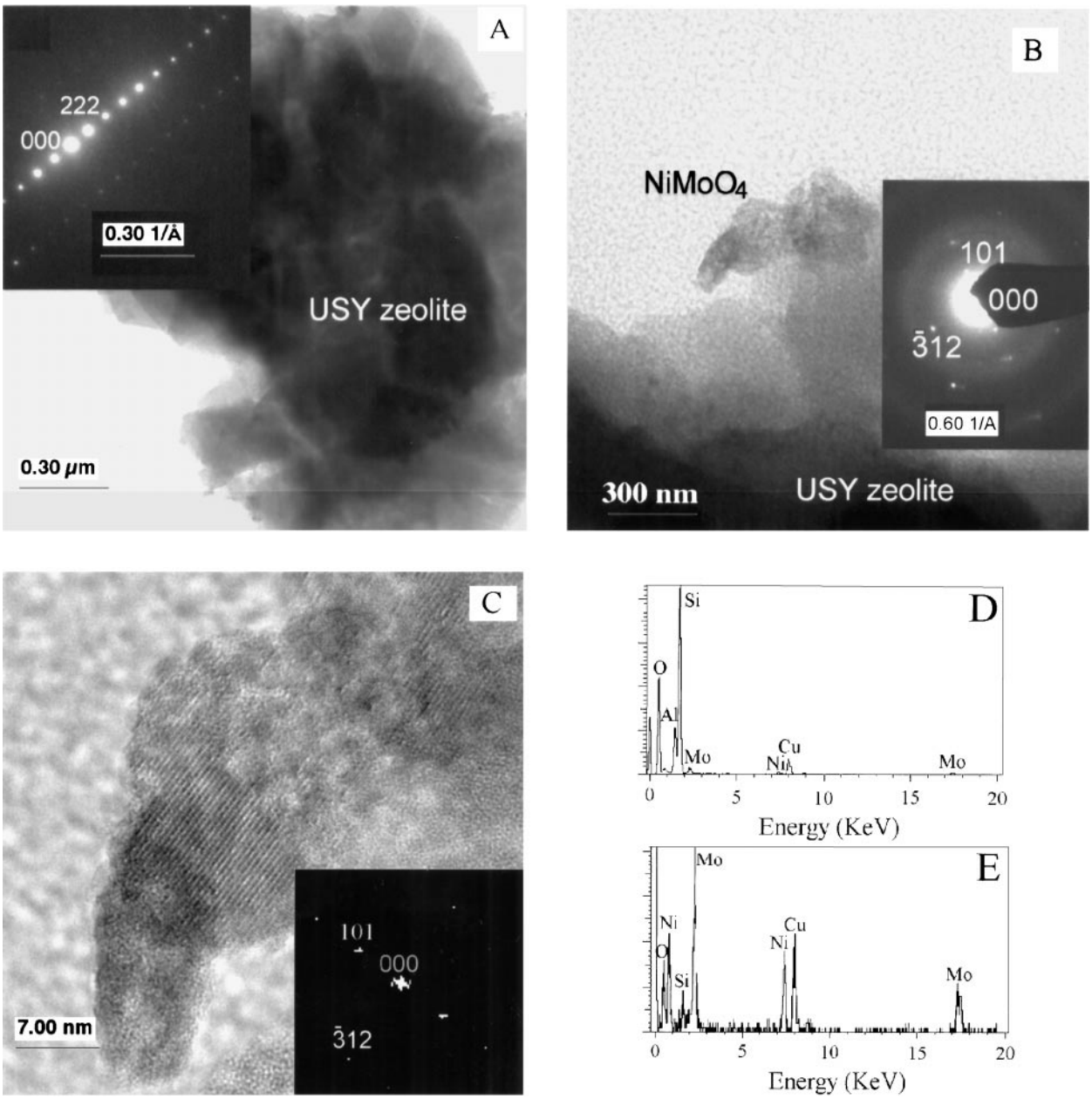

FIG. 1. (A) TEM image of zeolite in calcined Ni–Mo/USY catalyst, with an SAED pattern of USY shown in the inset. (B) TEM image of a Ni–Mo oxide particle attached to the surface of USY and its SAED pattern. (C) High-magnification image of the Ni–Mo oxide particle with the Fourier transform (indexed as α-$NiMoO_4$) of the image shown in the inset. (D) EDS analysis of the USY particle in Fig. 1A. (E) EDS analysis of the Ni–Mo oxide particle.

EDS analysis (Fig. 3D) of the Ni–Mo aggregates suggest that the Ni–Mo aggregates were α-$NiMoO_4$.

There was relatively a large number of small Ni–Mo sulfide aggregates on the surface of NaY zeolite in sulfided Ni–Mo/NaY (Fig. 4A). However, after a large number of NaY particles were surveyed, Ni–Mo sulfide aggregates in the sulfided catalyst appeared less abundant than the α-$NiMoO_4$ aggregates in the corresponding calcined precursor, probably because there were some large isolated Ni–Mo sulfide aggregates that were not able to attach on the surface of NaY, so were not observed in our sampling. EDS of NaY particles (Fig. 4C) showed the presence of Mo and possibly S, but very little Ni in NaY using a small spot of ~30 nm, which is essentially in agreement with calcined Ni–Mo/NaY and indicates that the sulfidation did not extensively affect Mo in NaY. The high-magnification image and EDS of the Ni–Mo sulfide aggregates are shown in Figs. 4B and 4D. The fringes were bending and the *d* spacing

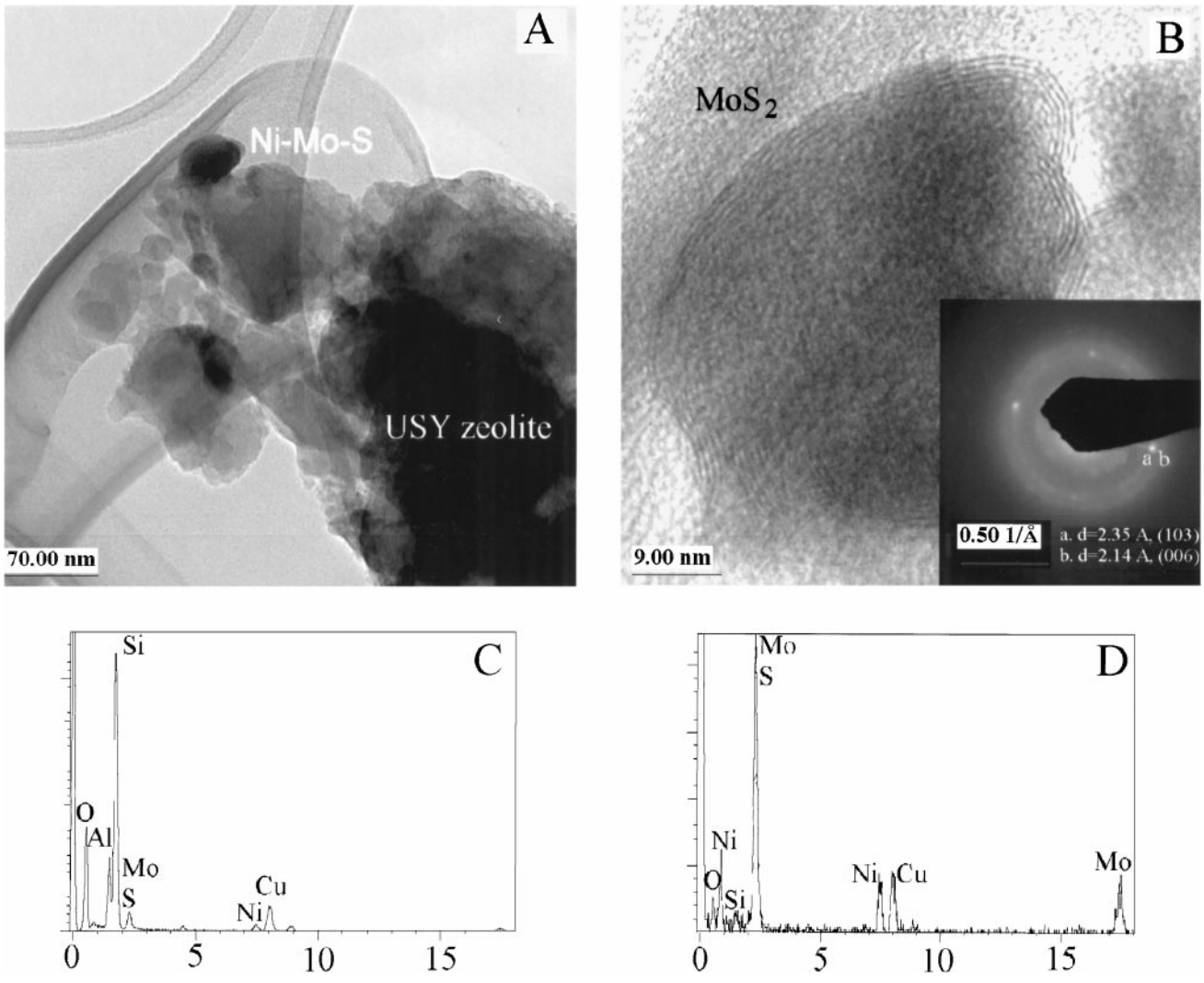

FIG. 2. (A) TEM image of a Ni–Mo sulfide aggregate on the surface of USY in a sulfide Ni–Mo/USY catalyst. (B) High-magnification image of the Ni–Mo sulfide particle. (C) EDS analysis of the USY zeolite particle in Fig. 2A. (D) EDS analysis of the Ni–Mo sulfide particle in Fig. 2B.

measured from the fringes was about 6.4 Å, close to the d_{002} of MoS_2 (6.15 Å). EDS shows that there were Mo and a small amount of Ni in the aggregates. As we argued before, because the S $K\alpha$ line and Mo L line were overlapped and the Ni–Mo/NaY was sulfided at 400°C and atmospheric pressure in which MoS_2 should be the most stable phase, thus, S should be present in the EDS and the aggregates might be MoS_2 containing some Ni.

Ni–Mo/mordenite

Mordenite was also well-crystallined as determined by SAED and bright-field imaging (Fig. 5A). EDS of mordenite shows essentially no Ni and very little Mo in mordenite. However, the contents of Ni and Mo detected by EDS varied largely, so that as an average of eight points, a small amount of both Ni and Mo was detected in mordenite particles by EDS (Table 2), probably because a number of small Ni–Mo oxide particles were disseminated on the mordenite particles. In addition, a large polycrystalline aggregate of α-$NiMoO_4$ was attached to a large crystal of MoO_3 (Fig. 5B). The SAED pattern and EDS analysis of the large crystal are shown in Figs. 5C and 5E, which clearly shows that this was a pure α-MoO_3. The high-magnification image and EDS analysis of the polycrystalline aggregate surrounding the α-MoO_3 crystal are shown in Figs. 5D and 5F, which indicate that this aggregate was monoclinic α-$NiMoO_4$.

After sulfidation, there were a large number of Ni and Mo aggregates on the surface of mordenite in sulfided Ni–Mo/mordenite, and essentially no Ni and Mo were detected by EDS in mordenite (Fig. 6A). Most interestingly, separate and intergrown Ni and Mo phases were observed (Fig. 6B). The fringes of the Mo phase were bending and surrounded the whole particles and the d spacing measured from the

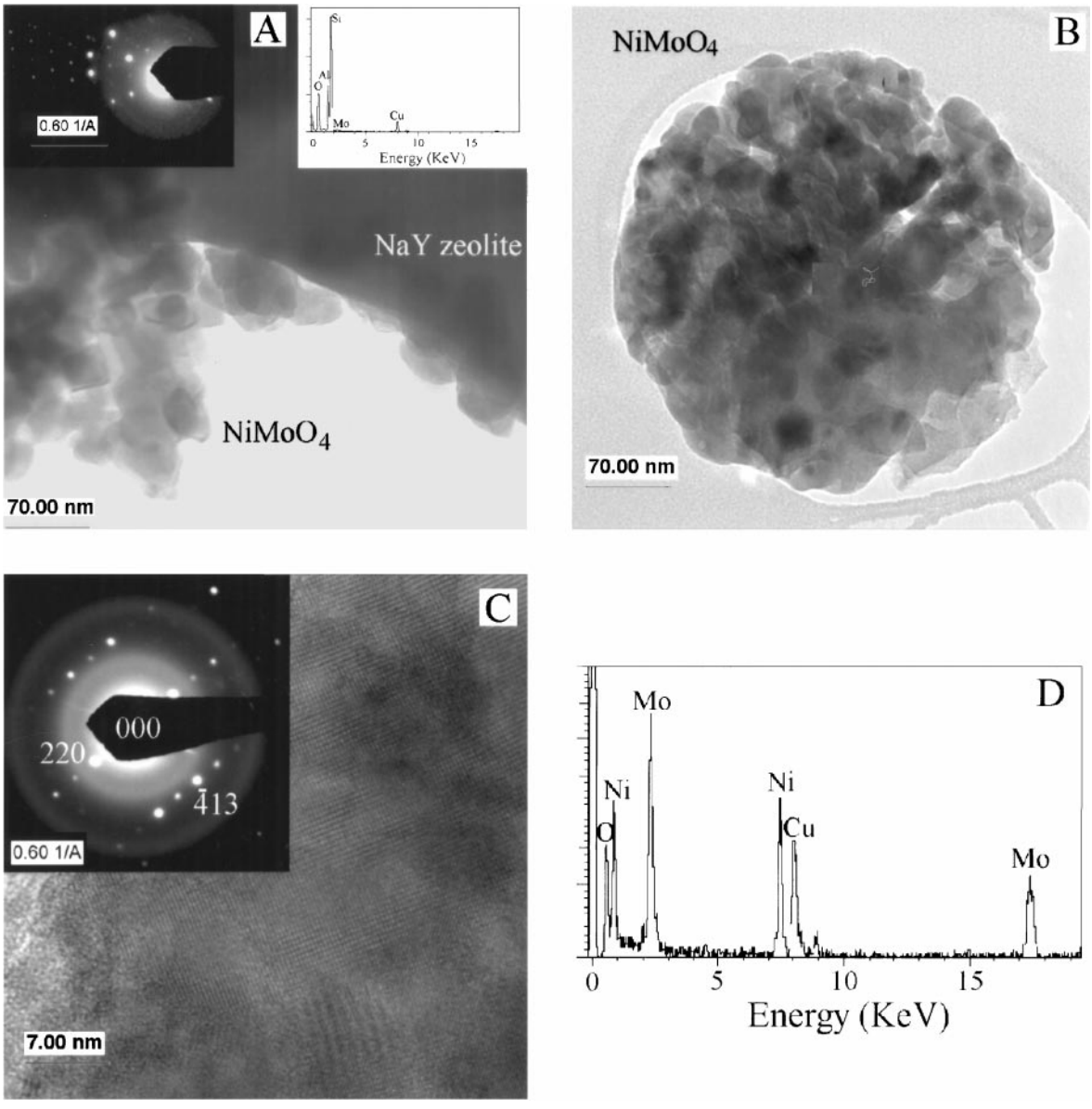

FIG. 3. (A) TEM image of NaY zeolite and Ni–Mo oxide aggregates in a calcined Ni–Mo/NaY zeolite catalyst, and an SAED pattern and EDS analysis of NaY are shown as insets. (B) TEM image of an isolated Ni–Mo oxide sphere, with a SAED pattern in the inset. (C) High-magnification TEM image and SAED pattern (in the inset) of a Ni–Mo oxide particle, and the SAED pattern was indexed based on α-$NiMoO_4$. (D) EDS analysis of Ni–Mo oxide particle.

fringes was about 6.3 Å, close to the d_{002} of MoS_2 (6.15 Å). EDS of the Mo phase appeared to be relatively pure MoS_2 because the S $K\alpha$ line and Mo L line were overlapped in EDS. The small amount of Ni detected by EDS may be due to the Ni in MoS_2 or the interference of the intergrowing Ni sulfide (Fig. 6D). The fringes of Ni sulfides were straight and the d spacing measured from the fringes was about 5.7 Å. The Ni sulfide appeared to be quite pure and the small amount of Mo in the EDS spectrum may be due to the interference by the surrounding MoS_2 (Fig. 6E). The SAED pattern of Ni sulfide was shown in Fig. 6C, in which the d spacings were calculated to be 5.9 and 2.4 Å, respectively, with an angle of about 90°. By reference to X-ray diffraction (XRD) data of all Ni sulfides, it was ruled out that this Ni sulfide was NiS with millerite structure (JCPDS 12-0041), Ni_3S_2 (JCPDS 30-0860), or NiS_2 (JCPDS 11-0099) which are normally believed to be stable at the sulfidation condition (400°C) because no d spacing of >5 Å is shown in the XRD data of these Ni sulfides. The XRD data for Ni_3S_4 (JCPDS 47-1739), α-Ni_7S_6 (JCPDS 24-1021), and Ni_9S_8 (JCPDS 22-1193) that has a d spacing close to 5.6 Å were also referred to, but it failed to index this SAED pattern. However, by

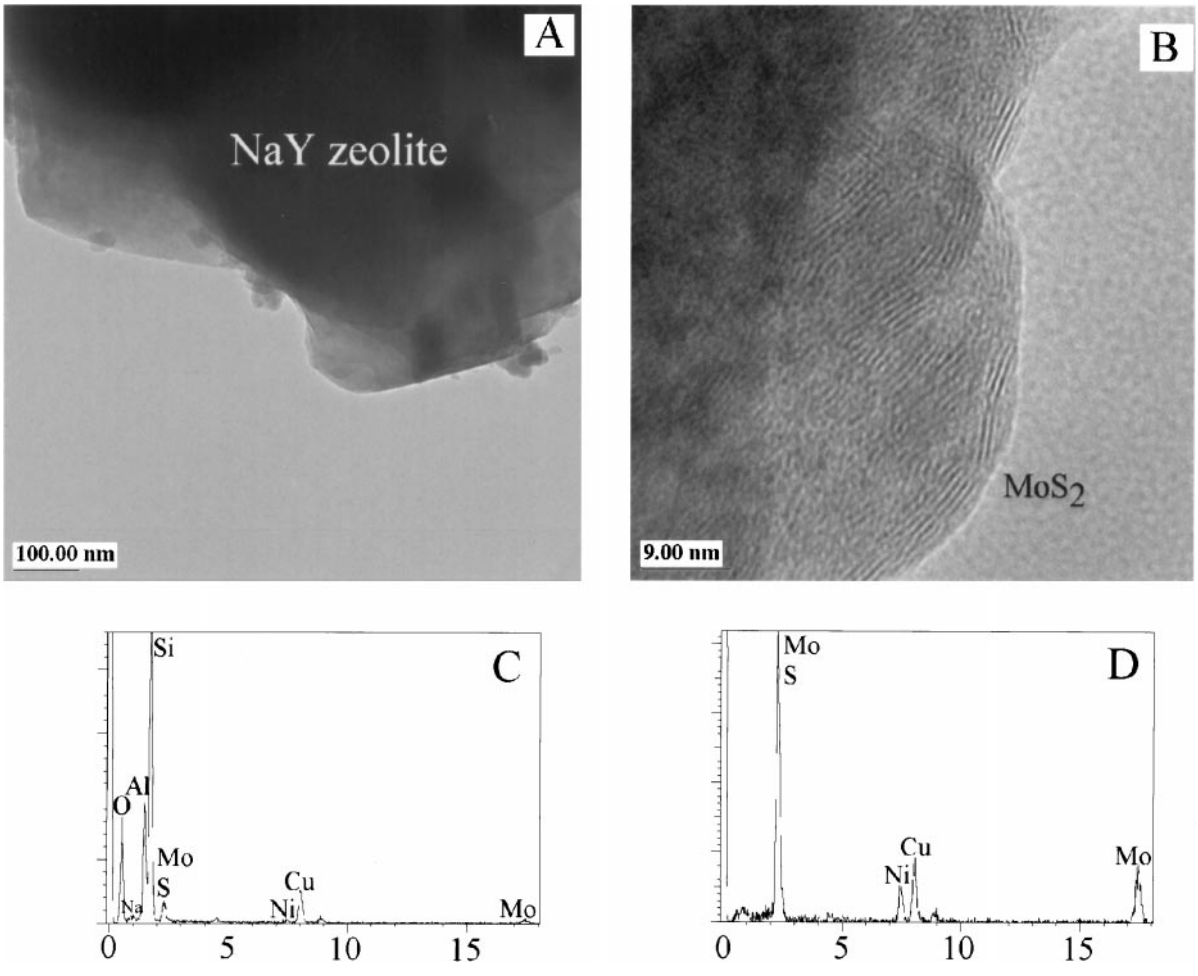

FIG. 4. (A) TEM image of NaY zeolite and small Ni–Mo sulfide particles attached on its surface in sulfided Ni–Mo/Nay catalyst. (B) High-magnification TEM image of Ni–Mo sulfide particles. (C) EDS analysis of NaY zeolite in Fig. 4A. (D) EDS analysis of Ni–Mo sulfide particle shown in Fig. 4B.

reference to XRD data of troilite or FeS (JCPDS 37-477), this pattern was nicely indexed (Fig. 6C). Thus, this Ni sulifde might be identified as troilite-like NiS. In fact, a similar phenomenon has also been observed for FeS_{1-x}: the most stable form of FeS_{1-x} is the pyrrhotite structure; however, the nanometer-sized FeS_{1-x} crystal produced by magnetotactic bacteria has the mackinawite (tetrogonal) structure (39).

Ni–Mo/ZSM-5

EDS analysis of ZSM-5 shows that no Ni and only a small amount of Mo were present in ZSM-5 (Fig. 7E), indicating that Ni and Mo were not significantly incorporated into the ZSM-5. Granular or needle Ni–Mo oxide aggregates formed on the surface of ZSM-5 (Figs. 7A and 7C), but an isolated needle Ni–Mo oxide aggregate was occasionally observed (Fig. 7B). The SAED patterns (the insets of Figs. 7A and 7B) of Ni–Mo oxides aggregates were indexed as α-$NiMoO_4$, as in the other Ni–Mo catalysts. The aggregates varied in length from 0.3 to about 2 μm. The high-magnification image and its Fourier transform (Fig. 7D) and EDS analysis of one aggregate particle (in Fig. 7F) also indicate that the aggregates were α-$NiMoO_4$.

In sulfided Ni–Mo/ZSM-5 catalyst, a very small amount of Mo and possibly S (due to the overlap of the S $K\alpha$ line and Mo L line in EDS), but no Ni, was detected in ZSM-5 by EDS (the inset of Fig. 8A), indicating the presence of Mo sulfide species in the lattice structure of ZSM-5. There were a large number of Ni and Mo sulfide aggregates on the surface of ZSM-5 (Fig. 8A), and these Ni and Mo sulfides were separate and intergrown (Fig. 8B). The fringes of Ni sulfide were straight and the d spacing measured from the fringes was about 5.6 Å (Figs. 8B and 8D); however, no high-quality SAED patterns were obtained to determine the entity of this Ni sulfide phase. The EDS spectrum of the Ni sulfide indicates that it was quite pure with the Ni/S ratio close to 1 (Fig. 8F). The EDS of the Mo phase again

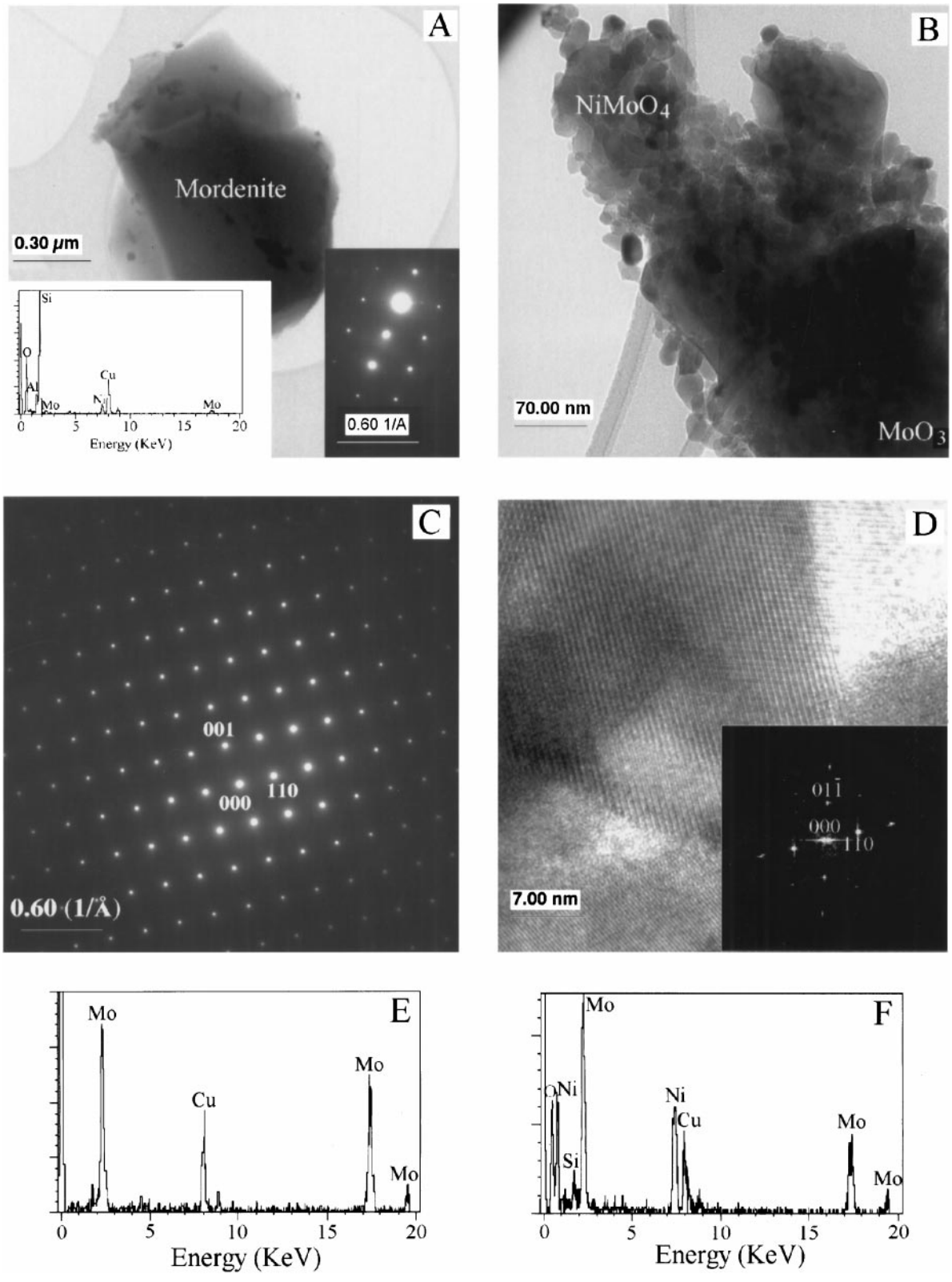

FIG. 5. (A) TEM image of mordenite and Ni–Mo oxide particles in calcined Ni–Mo/mordenite catalyst with an SAED pattern and EDS analysis shown as insets. (B) TEM image of a Ni–Mo oxide aggregate surrounding a large MoO_3 crystal. (C) SAED pattern of the MoO_3 crystal. (D) High-magnification image of a Ni–Mo oxide particle and its Fourier transform pattern (indexed as α-$NiMoO_4$) shown in the inset. (E) EDS analysis of the MoO_3 crystal. (F) EDS analysis of an Ni–Mo oxide particle.

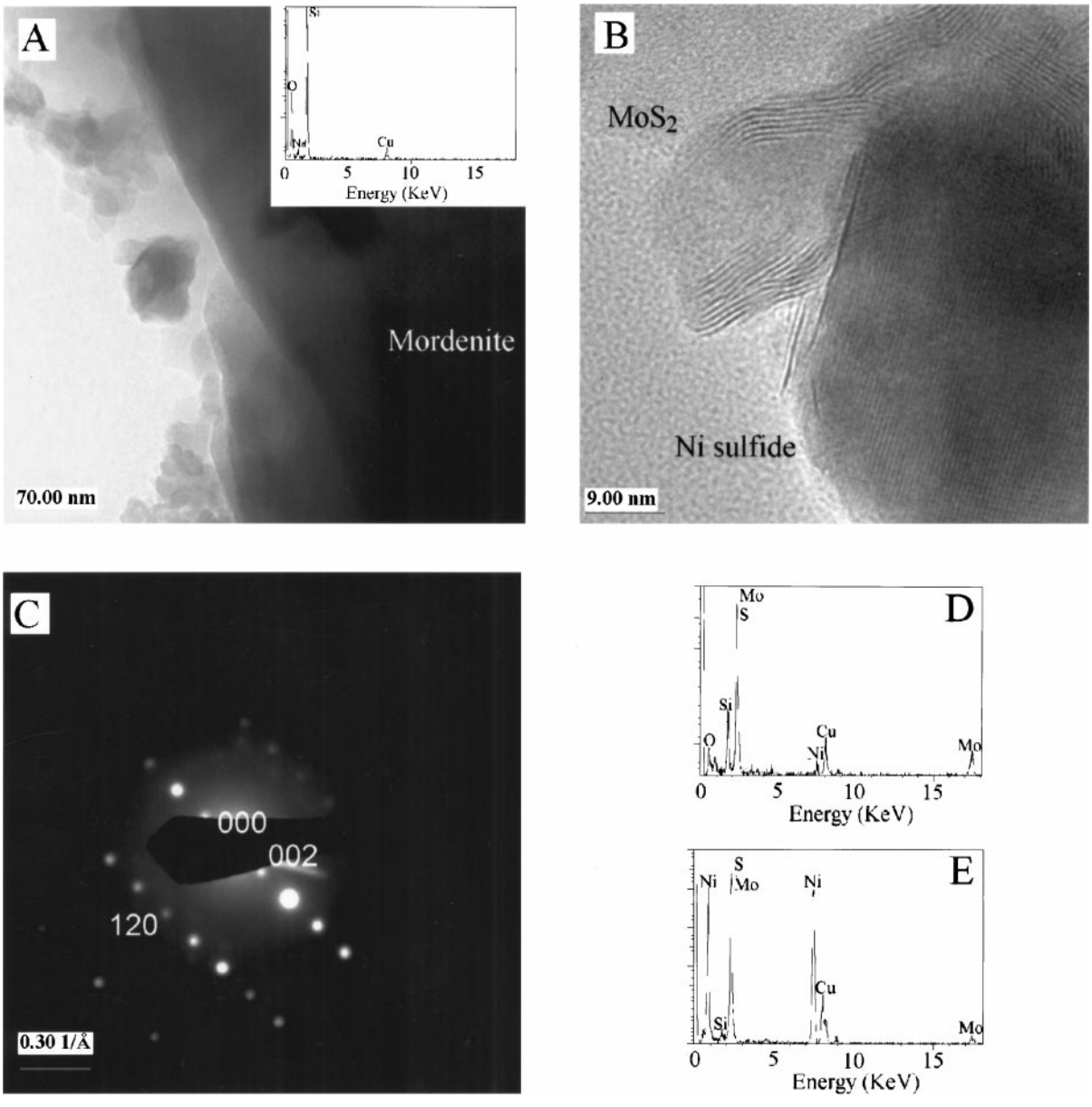

FIG. 6. (A) TEM image of mordenite and Ni and Mo sulfides attached on the surface of mordenite in sulfided Ni–Mo/mordenite catalyst, and EDS analysis of mordenite shown in the inset. (B) High-magnification TEM image of intergrown Ni and Mo sulfides. (C) SAED pattern of the Ni sulfide. (D) EDS analysis of the Mo sulfide particle. (E) EDS analysis of the Ni sulfide particle.

indicates that this phase might be a MoS_2 (S $K\alpha$ line and Mo L line were overlapped) containing some Ni (Fig. 8E). The fringes of the Mo sulfide were bending and surrounded the whole particle and the d spacing measured from the fringes was about 6.3 Å, close to the d_{002} of MoS_2 (6.15 Å). The SAED pattern (Fig. 8C) of the Mo phase was indexed based on XRD data of MoS_2 (JCPDS 37-1492). Thus, the Mo sulfide appeared to be MoS_2. The presence of a small amount of Ni in the EDS spectrum of the Mo sulfide may indicate that MoS_2 contained some Ni, but it may also be due to the effect of intergrown (as in Fig. 8B) Ni sulfide during EDS measurement.

DISCUSSION

Chemical States and Structures of Ni and/or Mo Species in Calcined Catalysts

The pH values of aqueous $Ni(NO_3)_2 \cdot 6H_2O$ and $(NH_4)_6Mo_7O_{24} \cdot 4H_2O$ solutions were not measured, but the co-aqueous solutions were expected to be neutral to slightly basic (17). At this pH range, USY, NaY, mordenite, and ZSM-5 are likely to have a slightly negative surface charge. In addition, each has a negatively charged internal framework. At this pH range, Ni^{2+} should be the dominant

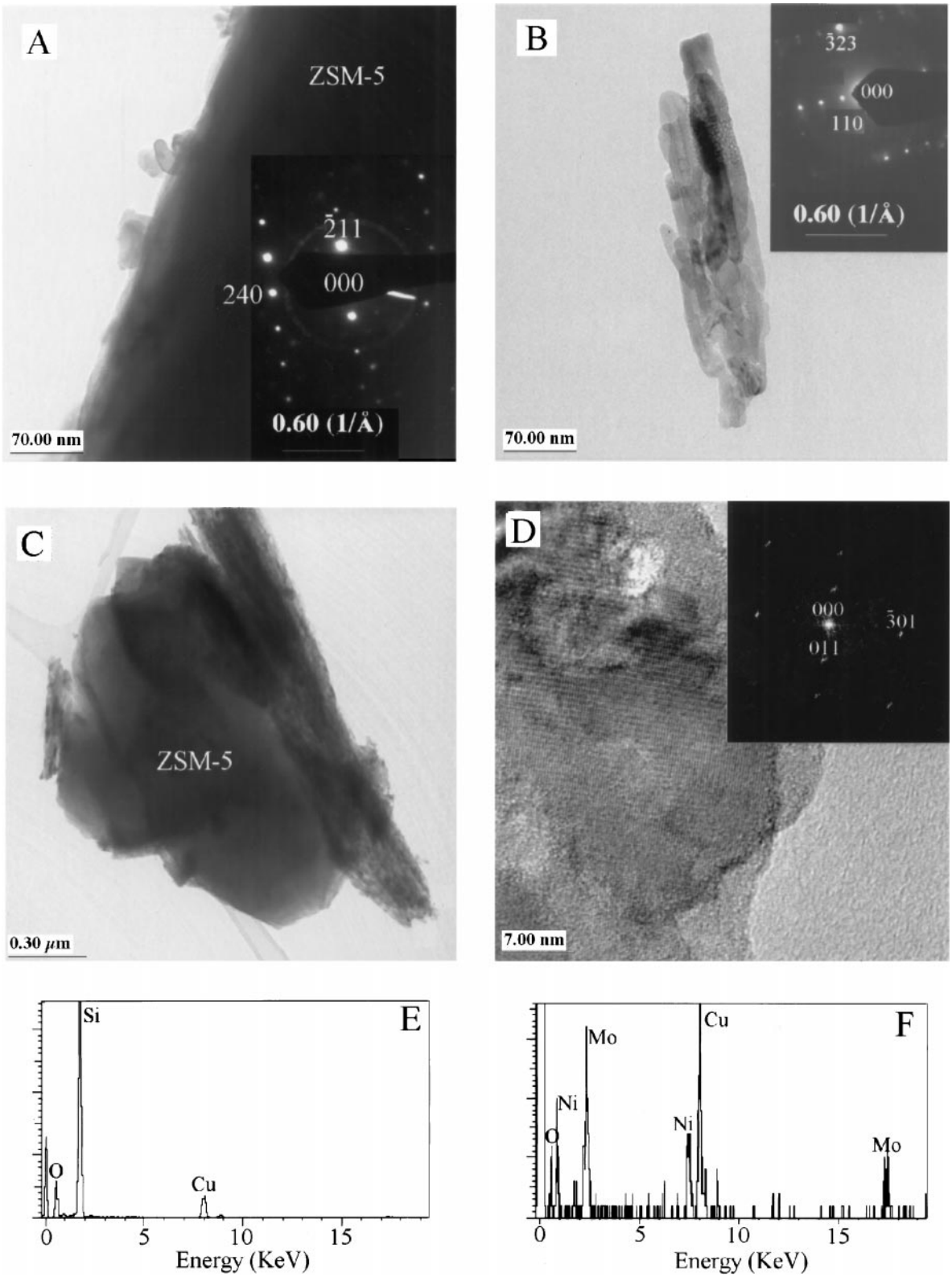

FIG. 7. (A) TEM image of ZSM-5 and Ni–Mo oxide particles attached on the surface of ZSM-5 in calcined Ni–Mo/ZSM-5 catalyst, and an SAED pattern (indexed as α-$NiMoO_4$) of one Ni–Mo oxide particle shown in the inset. (B) TEM image of an isolated needle Ni–Mo oxide aggregate with its SAED pattern (indexed as α-$NiMoO_4$) in the inset. (C) TEM image of ZSM-5 and two needle Ni–Mo oxide aggregates attached on the surface of ZSM-5. (D) High-magnification image and its Fourier transform (indexed as α-$NiMoO_4$ in the inset). (E) EDS analysis of a ZSM-5 particle shown in Fig. 7C. (F) EDS analysis of a Ni–Mo oxide particle shown in Fig. 7C.

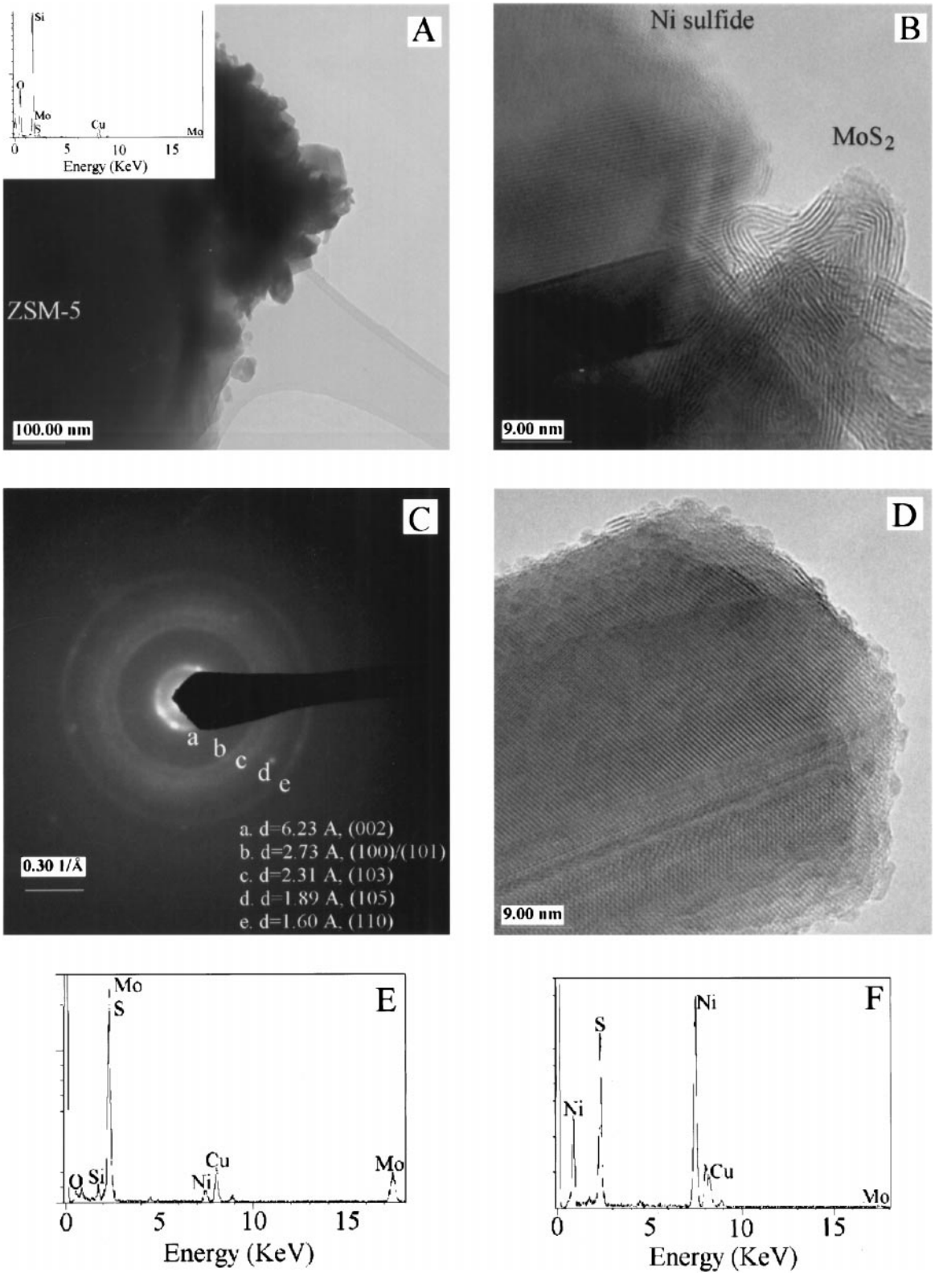

FIG. 8. (A) TEM image of ZSM-5 and Ni and Mo sulfide aggregates attached on the surface of ZSM-5 in sulfided Ni–Mo/ZSM-5 catalyst, with an EDS spectrum of ZSM-5 shown in the inset. (B) High-magnification TEM image of separate but intergrown Ni and Mo sulfide particles. (C) SAED pattern of MoS_2. (D) High-magnification image of a Ni sulfide particle. (E) EDS analysis of the Mo sulfide particle shown in Fig. 8B. (F) EDS analysis of the Ni sulfide particle shown in Fig. 8D.

Ni species (40, 41) and MoO_4^{2-} should be the dominant Mo species (41, 42). Based on the charge, Ni should have a strong electrostatic interaction with the surface and internal framework of these zeolites (i.e., it would be cation-exchanged). However, the electrostatic interaction of MoO_4^{2-} with the surface or the internal framework of these zeolites should be repulsive (i.e., it would not be cation-exchanged into zeolites). However, MoO_4^{2-} species may form inner-sphere complexes with the surface of the zeolites (42). During calcination, both Ni and Mo species may be re-distributed.

The final contents of NiO and MoO_3 in these catalysts (Table 2) were slightly below the loadings of NiO (2 wt%) and MoO_3 (8 wt%), indicating that some of the Ni and Mo was lost either at the ion-exchange stage or during the calcination. However, the molar NiO/MoO_3 ratio in these catalysts, except for Ni—Mo/mordenite, was close to about 0.48 (Table 2). The contents of NiO and MoO_3 in Ni–Mo/mordenite, analyzed by both INAA and EDS, were questionable, because the content of NiO determined by INAA was higher than 2 wt% and the content of NiO and MoO_3 determined by EDS was too high, considering the large number of $NiMoO_4$ and MoO_3 aggregates observed by TEM. Because very thin, transparent, and clean zeolite particles were chosen for EDS analysis, the NiO and MoO_3 detected by EDS were reasonably assumed to represent the total Ni and Mo in the zeolites. Thus, for Ni–Mo/USY, Ni–Mo/NaY, and Ni–Mo/ZSM-5, it is estimated that 50% of the total Mo and almost all Ni were incorporated into USY. Almost no Ni was detected in NaY and ZSM-5, but 40% and 66% of Mo were found in NaY and ZSM-5, respectively.

Based on the TEM observations, in Ni–Mo/USY, most of the Ni and Mo may be incorporated into the zeolite (e.g., supercavity and possibly sodalite cage), in good agreement with the fact that only one aggregate of Ni–Mo oxides was observed after a large number of USY particles were surveyed. In Ni–Mo/NaY and Ni–Mo/ZSM-5, Ni and Mo preferentially formed Ni–Mo oxide aggregates on the surface of the substrates or even formed isolated aggregates. However, because the Ni/Mo atomic ratio in the aqueous solutions was about 0.48, the excess Mo may be incorporated into NaY and ZSM-5. For Ni–Mo/mordenite, it is difficult to determine the relative proportions of Ni and Mo which may form Ni and Mo aggregates or be incorporated into mordenite because of the conflict between INAA and EDS. However, the contents of Ni and Mo determined semiquantitatively by EDS may be too high since some Ni and Mo oxide aggregates of nanometer size were disseminated in mordenite particles (Fig. 5A).

MoO_3 crystals were observed in Ni–Mo/mordenite, which were identified by SAED as α-MoO_3. The MoO_3 crystals were often surrounded by Ni–Mo oxide aggregates. However, MoO_3 was not observed in Ni–Mo/USY, Ni–Mo/NaY, and Ni–Mo/ZSM-5 by HRTEM. Most of the aggregates in all of these catalysts were identified by EDS as Ni–Mo oxides with the Ni/Mo atomic ratio normally being ≤ 1, but occasionally >1. Regardless of the Ni/Mo atomic ratio, the Ni–Mo oxide aggregates were identified by SAED as monoclinic α-$NiMoO_4$. The Ni/Mo ratio changed largely for different aggregates, indicating that the α-$NiMoO_4$ aggregates are nonstoichiometric. A pure NiO phase was not found by EDS or SAED in any of the zeolite-supported Ni–Mo catalyst precursors.

Chemical States and Structures of Ni and/or Mo Species in Sulfide Catalysts

In sulfided Ni–Mo/USY catalyst (Ni–Mo/USY-(S)), only one Ni–Mo sulfide particle was found on the surface of USY zeolite after a large number of USY particles were surveyed. Based on the *d* spacing measured from the fringes, it was MoS_2. However, EDS shows that some Ni may be present in MoS_2; thus, the Ni–Mo sulfide aggregate was possibly so-called Ni–Mo–S phase (43). Because Ni–Mo sulfide aggregates were rarely observed in Ni–Mo/USY-(S), it is speculated that sulfidation did not extensively affect Ni and Mo that have been incorporated into the supercavity or sodalite cage of USY in calcined Ni–Mo/USY, and most of the Ni and Mo may have formed Ni–Mo sulfide species in the supercavity (and possibly in the sodalite cage). In sulfided Ni–Mo/NaY catalyst (Ni–Mo/NaY-(S)), there were a large number of small Ni–Mo sulfide aggregates on the surface of NaY. As in Ni–Mo/USY-(S), the Ni–Mo aggregates were MoS_2 containing some Ni. However, some MoS_2 species may also have formed in the lattice structure of NaY zeolite, although the current TEM was not able to observe it.

In sulfided Ni–Mo/mordenite (Ni–Mo/mordenite-(S)) and Ni–Mo/ZSM-5 catalysts (Ni–Mo/ZMS-5-(S)), there were a large number of Ni and Mo sulfides on the surface of the substrates. The MoS_2 species contains much less Ni and appeared quite close to pure MoS_2; however, a Ni sulfide phase was extensively observed. The Ni sulfide phase is very small in size (normally ~40–50 nm) and may have roughly a Ni/S ratio of 1 : 1 without much Mo. Although Mo was detected in the EDS of the Ni sulfide, it may be due to the interference of intergrowing MoS_2. The structure of this Ni sulfide was not fully understood. However, it can be ruled out that it was NiS with millerite structure, Ni_3S_2 or Ni_3S_2, although the former two Ni sulfides are normally stable thermodynamically and are believed to be present in sulfided Ni/Al_2O_3 catalyst (43). This Ni sulfide in Ni–Mo/mordenite-(S) appeared not to be Ni_3S_4, Ni_7S_6, or Ni_9S_8 because the SAED pattern can not be indexed based on the XRD data of these Ni sulfides, but might be NiS with a troilite structure. The troilite-like NiS has not been reported yet to the best of our knowledge. If this is true, it may indicate that Ni speciation at nanometer size as in Ni and Ni–Mo sulfide catalysts may not be predicted simply based on macroscopic thermodynamics. In Ni–Mo/ZSM-5-(S), the entity of

the Ni sulfide can not be determined simply based on the high-magnification image and the *d* spacing of about 5.6 Å, which is observed in the XRD of α-Ni_7S_6, Ni_9S_8, and NiS with a troilite structure.

By comparison of TEM observation of both calcined and sulfide Ni–Mo catalysts, it appears that sulfidation does not affect extensively the Ni and Mo incorporated into the lattice structure of zeolite. Qualitatively, the more Ni and/or Mo oxide aggregates were present on the surface of zeolites in calcined precursors, the more Ni and/or Mo sulfide aggregates were observed in the corresponding sulfided catalysts. Thus, it can be believed that Ni and/or Mo oxide aggregates (mainly α-$NiMoO_4$; MoO_3 was observed only in calcined Ni–Mo/mordenite) on the surface of zeolites are transformed into the corresponding Ni and/or Mo sulfides by sulfidation. However, the structure and composition of the substrates also exert an important influence on the Ni speciation in Ni–Mo sulfide catalysts. For example, in Ni–Mo/USY and Ni–Mo/NaY catalysts, $NiMoO_4$ is mainly transformed into MoS_2 containing some Ni or so-called Ni–Mo–S phase, as in Ni–Mo/Al_2O_3 catalyst (43); however, $NiMoO_4$ is transformed into separate and intergrown MoS_2 and Ni sulfide phases. The major sulfidation reactions are described as follows:

$$MoO_3 + 2H_2S + H_2 \leftrightarrow MoS_2 + 3H_2O, \quad [1]$$

$$NiMoO_4 + H_2S + H_2 \rightarrow Ni\text{–}Mo\text{–}S + H_2O, \quad [2]$$

$$NiMoO_4 + 3H_2S + H_2 \leftrightarrow MoS_2 + NiS + 4H_2O. \quad [3]$$

Reaction [2] is not balanced because the chemical stoichiometry of the so-called Ni–Mo–S phase is not accurately known (43). Reaction [2] is a major sulfidation reaction for Ni–Mo/USY and Ni–Mo/NaY catalysts; reactions [1] and [3] occur in the sulfidation of Ni–Mo/mordenite; and reaction [3] may be responsible for the sulfidation of the Ni–Mo/ZSM-5 catalyst.

Chemical States and Structures of Ni and Mo Species versus HDS Catalytic Activity

The HDS activity data (in both wt% and $\times 10^8$ mmol/(m^2 s)) for dibenzothiophene over Ni–Mo/USY-(S), Ni–Mo/NaY-(S), Ni–Mo/mordenite-(S), Ni–Mo/ZSM-5-(S), and the untreated zeolite supports are given in Table 1. Ni–Mo/USY-(S) has much higher HDS activity than Ni-Mo/NaY-(S), Ni–Mo/mordenite-(S), and Ni–Mo/ZSM-5-(S). The high HDS activity of Ni–Mo/USY-(S) is closely related to that of the Ni–Mo–S species in the lattice structure (e.g., the supercavity) of USY, as well as the Brønsted acidity of USY (17). In particular, the Ni and Mo species in the supercavity of USY may form a Ni–Mo–S phase during sulfidation, and the Ni–Mo–S phase in the supercavity is the major active phase for the HDS of dibenzothiophene. Both the Ni–Mo–S active phase and Brønsted acidity in Ni–Mo/USY-(S) may have synergistic effect on the HDS reaction.

The HDS activity of Ni–Mo/NaY-(S) is higher than that of NaY, but significantly lower than that of Ni–Mo/USY-(S). First, NaY has no Brønsted acid site (17). Second, Ni and Mo preferentially formed α-$NiMoO_4$ both on the surface of NaY and as isolated particles, causing the Ni and Mo to be poorly dispersed and a large number of Ni–Mo sulfide aggregates to be formed in the Ni–Mo/NaY-(S) catalyst. Third, an excess of Mo (not incorporated into the α-$NiMoO_4$ particles) may have been incorporated into NaY (e.g., the sodalite cage) during calcination, making the Mo inaccessible to dibenzothiophene. Thus, Ni–Mo/NaY-(S) has a much lower HDS activity than Ni–Mo/USY-(S).

The HDS activities of Ni–Mo/mordenite-(S) and Ni–Mo/ZSM-5-(S) are also significantly lower than that for Ni–Mo/USY-(S) because most of the Ni and Mo was incorporated into α-$NiMoO_4$ or α-MoO_3, causing the Ni and Mo to be poorly dispersed and, hence, poorly sulfided in the final catalysts. After sulfidation, separate and intergrown MoS_2 and Ni sulfide are formed on the surface of the substrates; these two sulfides have low specific HDS activity. Thus, the HDS activities of Ni–Mo/mordenite-(S) and Ni–Mo/ZSM-5-(S) are not significantly greater than their corresponding zeolites.

Our TEM observations of Ni–Mo/NaY and Ni–Mo/USY are, to some extent, at odds with previous observations (15, 36). For example, Leglise *et al.* (15) found that Ni but only half of the Mo enter HY zeolites. The other half of the Mo forms MoO_3 outside the HY zeolite grains, and Ni–Mo oxide is far less common than MoO_3. The sulfidation transforms the outside MoO_3 into MoS_2 and evicts half of the Ni in the cavity to form a Ni–Mo–S phase that is responsible for the high hydrogenation activity for benzene over Ni–Mo/HY-(S). However, our TEM results suggest that the α-$NiMoO_4$ phase is a major Ni–Mo oxide phase in all calcined catalysts studied; MoO_3 is observed only in calcined Ni–Mo/mordenite. Ni and Mo were mainly located within USY (e.g., in the supercavity sites); sulfidation does not significantly affect the Ni and Mo incorporated into the supercavity of USY zeolite. Thus, the Ni and Mo were sulfided to form Ni–Mo–S species in the supercavity of USY. Welter *et al.* (36–38) argued that although there are some Ni–Mo aggregates on the surface of NaY, only the small Ni–Mo sulfide clusters in the NaY zeolite supercavity strongly contribute to the thiophene HDS activity. However, in our sample of Ni–Mo/NaY, Ni and Mo were largely distributed outside of NaY in the form of α-$NiMoO_4$, making them difficult to be sulfided and not finely disseminated. In addition, very little Ni, but a small amount of Mo, may have been incorporated into the sodalite cage, but not the supercavity of NaY. The sodalite cage is too small to be accessed by dibenzothiophene molecules. Thus, the HDS activity for dibenzothiophene over Ni–Mo/NaY-(S) is quite low. The active phase responsible for the HDS of dibenzothiophene

is the so-called Ni–Mo–S phase located in the supercavity of USY, and the Ni–Mo–S phase, MoS_2, and Ni sulfide on the surface of zeolite do not significantly contribute to the HDS activity of dibenzothiophene. In fact, the combination of the Ni–Mo–S phase and Brønsted acidity in the supercavity (as in Ni–Mo/USY-(S)) is very essential for high HDS activity of dibenzothiophene. Of course, the discrepancies between our current observations and the previous results in the literature may also be due to different sample preparations; e.g., aqueous ion exchange was used in our sample preparation, but Leglise *et al*. (13–15) used a sequential impregnation.

CONCLUSIONS

In Ni–Mo/USY, both Ni and Mo were incorporated into the lattice structure (e.g., the supercavity) of USY, and Ni–Mo oxide aggregates were rarely found by HRTEM. During sulfidation, Ni and Mo were not extensively evicted from the lattice structure of USY zeolite, and Ni and Mo species were sulfided to form Ni–Mo–S clusters. The Ni–Mo–S clusters in the supercavity of USY zeolite and Brønsted acid sites synergetically contribute to produce the high HDS activity of dibenzothiophene. For Ni–Mo/NaY, Ni–Mo/mordenite, and Ni–Mo/ZSM-5, Ni and Mo preferentially form α-$NiMoO_4$ aggregates, and the excess of Mo may be incorporated into the lattice structure or form MoO_3 (as seen only in Ni–Mo/mordenite) during calcination. The formation of α-$NiMoO_4$ aggregates caused the distribution of the Ni and Mo to be poorly dispersed and poorly sulfided. In sulfided Ni–Mo/NaY catalysts, the major Ni–Mo sulfide species on the surface of NaY zeolite was MoS_2 containing some Ni; while in sulfided Ni–Mo/mordenite and Ni–Mo/ZSM-5 catalysts, separate and intergrown Ni sulfide and MoS_2 were observed, although the entity of the Ni sulfide has not been fully understood. Although some MoS_2 species may have formed in the lattice structure of NaY, mordenite, and ZSM-5, it was not a major active species for the HDS of dibenzothiophene. In addition, the Brønsted acidity of Ni–Mo/USY zeolite catalysts is very high (17); the combination of the active Ni–Mo–S species formed in the supercavity (and possibly in the sodalite cage) and the high Brønsted acidity in Ni–Mo/USY zeolite catalyst contribute to very high HDS of dibenzothiophene. However, sulfided Ni–Mo/NaY, Ni–Mo/mordenite, and Ni–Mo/ZSM-5 catalysts have very low Brønsted acidity, and the major Ni and/or Mo species were MoS_2 containing some Ni, or even separate, Ni and Mo sulfide phases on the surface of the substrates; thus, these catalysts had very low HDS activity of dibenzothiophene.

ACKNOWLEDGMENTS

We thank Y. Kanda, T. Sato, and A. Nishijima in the National Institute of Materials and Chemical Research, Japan, for their assistance with sulfidation, and J. W. Carey, Los Alamos National Laboratory, for his thorough review of this manuscript.

REFERENCES

1. Maxwell, I. E., *Catal. Today* **1**, 385 (1987).
2. Baudon, A., Lemberton, J. L., Guisnet, M., Marchal, N., and Mignard, S., *Catal. Lett.* **36**, 245 (1996).
3. Vazquez, M. I., Escardino, A., and Corma, A., *Ind. Eng. Chem. Res.* **26**, 1495 (1987).
4. Welters, W. J. J., van der Waerden, O. H., de Beer, V. H. J., and van Santen, R. A., *Ind. Eng. Chem. Res.* **34**, 1166 (1995).
5. Cid, R., Orellana, F., and Lopez Agudo, A., *Appl. Catal.* **32**, 327 (1987).
6. Corma, A., Vazquez, M. I., Bianconi, A., Clozza, A., Garcia, J., Pallota, O., and Cruz, G. M., *Zeolites* **8**, 464 (1988).
7. Spojakina, A. A., and Kostova, N., *Collect. Czech. Chem. Commun.* **57**, 2509 (1992).
8. Okamoto, Y., and Katsuyama, H., *Stud. Surf. Sci. Catal.* **101**, 503 (1996).
9. Okamoto, Y., and Katsuyama, H., *AIChE J.* **43**, 2809 (1997).
10. Kovacheva, P., Davidova, N., and Novakova, J., *Zeolites* **11**, 54 (1991).
11. Tatsumi, T., Taniguchi, M., Ishige, H., Ishii, Y., Murata, T., and Hidai, M., *Appl. Catal.* **121/122**, 500 (1997).
12. Cid, R., Gil Llambias, F. J., Gonzalez, M., and Lopez Agudo, A., *Catal. Lett.* **24**, 147 (1994).
13. Leglise, J., Janin, A., Lavalley, J. C., and Cornet, D., *J. Catal.* **114**, 388 (1988).
14. Leglise, J., el Qotbi, M., Goupil, J. M., and Cornet, D., *Catal. Lett.* **10**, 103 (1991).
15. Leglise, J., Manoli, J. M., Potvin, C., Djega-Mariadassou, G., and Cornet, D., *J. Catal.* **152**, 275 (1995).
16. Vasudevan, P. T., and Fierro, J. L. G., *Catal. Rev.-Sci. Eng.* **38**, 161 (1996).
17. Li, Dien Nishijima, A., and Morris, D. E., *J. Catal.* **182**, 339 (1999).
18. Sanders, J. V., and Pratt, K. C., *J. Catal.* **67**, 331 (1981).
19. Delannay, F., *Appl. Catal.* **16**, 135 (1985).
20. Hayden, T. F., Dumesic, J. A., Sherwood, R. D., and Baker, T. K., *J. Catal.* **105**, 299 (1987).
21. van Doorn, J., Moulijn, J. A., and Djéga-Mariadassou, G., *Appl. Catal.* **63**, 77 (1990).
22. Smith, B. J., and Wei, J., *J. Catal.* **132**, 21 (1991).
23. Smith, B. J., and Wei, J., *J. Catal.* **132**, 41 (1991).
24. Cruz-Reyes, J., Avalos-Borja, M., Farías, M. H., and Fuentes, S., *J. Catal.* **137**, 232 (1992).
25. Srinivasan, S., and Datye, A. K., *J. Catal.* **137**, 513 (1992).
26. Eijsbouts, S., Heinerman, J. J. L., and Elzerman, H. J. W., *Appl. Catal. A* **105**, 53 (1993).
27. Eijsbouts, S., Heinerman, J. J. L., and Elzerman, H. J. W., *Appl. Catal. A* **105**, 69 (1993).
28. Eijsbouts, S., *Appl. Catal. A* **158**, 53 (1998).
29. Aksoylu, A. E., Misirli, Z., and Onsan, Z. I., *Appl. Catal. A* **168**, 385 (1998).
30. Calais, C., Matsubayashi, N., Geantet, C., Yoshimura, Y., Shimada, H., Nishijima, A., Lacroix, M., and Breysse, M., *J. Catal.* **174**, 130 (1998).
31. Okamoto, Y., Nagata, K., Adachi, T., Imanaka, T., Imamura, K., and Takyu, T., *J. Phys. Chem.* **95**, 310 (1991).
32. de Boer, M., van Dillen, A. J., Koningsberger, D. C., and Geus, J. W., *J. Phys. Chem.* **98**, 7862 (1994).
33. Díaz, A., Acosta, D. R., Odriozola, J. A., and Montes, M., *J. Phys. Chem.* **101**, 1782 (1997).
34. Prinetto, F., Cerrato, G., Ghiotti, G., Chiorino, A., Campa, M. C., Gazzoli, D., and Indovina, V., *J. Phys. Chem.* **99**, 5556 (1995).

35. Cid, R., Gil Llambías, F. J., Fierro, J. L. G., López Agudo, A., and Villaseñor, J., *J. Catal.* **89**, 478 (1984).
36. Welters, W. J. J., Vorbeck, G., Zandbergen, H. W., de Haan, J. W., de Beer, V. H. J., and van Santen, R. A., *J. Catal.* **150**, 155 (1994).
37. Welters, W. J. J., van der Waerden, O. H., Zandbergen, H. W., de Beer, V. H. J., and van Santen, R. A., *Ind. Eng. Chem. Res.* **34**, 1156 (1995).
38. Welters, W. J. J., van der Waerden, O. H., de Beer, V. H. J., and van Santen, R. A., *Ind. Eng. Chem. Res.* **34**, 1166 (1995).
39. Posfai, M., Buseck, P. R., Bazylinski, D. A., and Frankel, R. B., *Science* **280**, 880 (1998).
40. Vordonis, L., Spanos, N., Koutsoukos, P. G., and Lycourghiotis, A., *Langmuir* **8**, 1736 (1992).
41. Spanos, N., and Lycourghiotis, A., *J. Colloid Interface Sci.* **171**, 306 (1995).
42. Spanos, N., and Lycourghiotis, A., *J. Catal.* **147**, 57 (1994).
43. Topsoe, H., Clausen, B. S., and Massoth, F. E., "Hydrotreating Catalysis: Science and Technology," p. 310. Springer-Verlag, Berlin, 1996.